

Wigner function quantum molecular dynamics

Vladimir Filinov^{1,2}, Michael Bonitz², Alexei Filinov², and Volodymyr Golubnychiy²

¹ Institute for High-Energy Density, Russian Academy of Sciences, Moscow 127412, Russia

² Institut für Theoretische Physik und Astrophysik, Christian-Albrechts-Universität, 24098 Kiel

1.1 Introduction

Classical molecular dynamics (MD) is a well established and powerful tool in various fields of science, e.g. chemistry, plasma physics, cluster physics and condensed matter physics. Objects of investigation are few-body systems and many-body systems as well. The broadness and level of sophistication of this technique is documented in many monographs and reviews, see for example [1, 2, 3]. Here we discuss the extension of MD to quantum systems (QMD). There have been many attempts in this direction which differ from one another, depending on the type of system under consideration. One direction of QMD has been developed for condensed matter systems and will not be discussed here, e.g. [4]. In this chapter we are dealing with unbound electrons as they occur in gases, fluids or plasmas. Here, one strategy is to replace classical point particles by wave packets, e.g. [4, 5, 6] which is quite successful. At the same time, this method struggles with problems related to the dispersion of such a packet and difficulties to properly describe strong electron-ion interaction and bound state formation. We, therefore, avoid such restrictions and consider a completely general alternative approach. We start discussion of quantum dynamics from a general consideration of quantum distribution functions.

1.2 Quantum distribution functions

There exists a variety of different representations of quantum mechanics including the so-called *Wigner representation* which involves a class of functions depending on coordinates and momenta. In the classical limit, the Wigner distribution F^W turns into the phase space distribution f known from classical statistical mechanics. In contrast to f , the Wigner function may be non-positive which is a consequence of the coordinate-momentum (Heisenberg) uncertainty. This will lead to a modification of particle trajectories which we

discuss below in Sec. 1.4. An important property of the distribution functions is that they can be used to compute the expectation value of an arbitrary physical observable, $\langle A \rangle$, defined by the operator $\hat{A}(\hat{p}, \hat{q})$ [7],

$$\langle A \rangle(t) = \int dpdq A^W(p, q) F^W(p, q, t), \quad 1 = \int dpdq F^W(q, p, t), \quad (1.1)$$

where $A^W(p, q)$ is a scalar function and, for simplicity, we consider the 1D case (generalization to higher dimensions and N particles is straightforward by re-defining the coordinate and momentum as vectors, $q = \{\mathbf{q}_1, \dots, \mathbf{q}_N\}$, $p = \{\mathbf{p}_1, \dots, \mathbf{p}_N\}$). F^W is defined via the nonequilibrium N -particle density operator $\hat{\rho}$ in coordinate representation (i.e. the density matrix),

$$F^W(p, q, t) = \frac{1}{2\pi\hbar} \int d\nu \left\langle q + \frac{\nu}{2} | \hat{\rho} | q - \frac{\nu}{2} \right\rangle e^{-i\nu p}, \quad (1.2)$$

and $A^W(p, q)$ is analogously defined from the coordinate representation of \hat{A} .

We now consider the time evolution of the WF under the influence of a general hamiltonian of the form

$$\hat{H} = \sum_{j=1}^N \frac{\hat{p}_j^2}{2m} + \sum_{i=1}^N \tilde{V}(q_i) + \sum_{i<j} V(q_i, q_j), \quad (1.3)$$

where $\tilde{V}(q_i)$ and $V(q_i, q_j)$ denote an external and an interaction potential, respectively. The equation of motion of F^W has the form [8, 7], some explanations are given in Sec. 1.4,

$$\frac{\partial F^W}{\partial t} + \frac{\mathbf{p}}{m} \cdot \nabla_q F^W = \int_{-\infty}^{\infty} ds F^W(p-s, q, t) \tilde{\omega}(s, q, t), \quad (1.4)$$

where the function

$$\tilde{\omega}(s, q, t) = \frac{2}{\pi\hbar^2} \int dq' V(q-q', t) \sin\left(\frac{2sq'}{\hbar}\right) \quad (1.5)$$

takes into account the non-local contribution of the potential energy in the quantum case. Equivalently, expanding the integral around $q' = 0$, Eq. (1.4) can be rewritten with an infinite sum of local potential terms

$$\frac{\partial F^W}{\partial t} + \frac{p}{m} \frac{\partial F^W}{\partial q} = \sum_{n=0}^{\infty} \frac{(\hbar/2i)^{2n}}{(2n+1)!} \left(\frac{\partial^{2n+1} V}{\partial q^{2n+1}}, \frac{\partial^{2n+1} F^W}{\partial p^{2n+1}} \right), \quad (1.6)$$

where (\dots, \dots) denotes the scalar product of two vectors which for an N -particle system contain $3N$ components.

If the potential does not contain terms higher than the second power of q , i.e. $\frac{\partial^n V}{\partial q^n} |_{n \geq 3} = 0$, then Eq. (1.6) is simplified and reduces to the classical Liouville equation for the distribution function f , i.e.

$$\frac{\partial f}{\partial t} + \frac{p}{m} \frac{\partial f}{\partial q} = \frac{\partial V}{\partial q} \frac{\partial f}{\partial p}. \quad (1.7)$$

The Wigner function must satisfy a number of conditions [9], therefore, the initial function $F^W(q, p, 0)$ cannot be chosen arbitrarily. Even if $F^W(q, p, t)$ satisfies the classical equation (1.7) it nevertheless describes the evolution of a quantum distribution because a properly chosen initial function $F^W(q, p, 0)$ contains, in general, all powers of \hbar . In particular, the uncertainty principle holds for average values of operators calculated with $F^W(q, p, 0)$ and $F^W(q, p, t)$.

One can rewrite Eq. (1.6) in the form analogous to the classical equation (1.7) by replacing V by a new effective potential V_{eff} defined as

$$\frac{\partial V_{\text{eff}}}{\partial q} \frac{\partial F^W}{\partial p} = \frac{\partial V}{\partial q} \frac{\partial F^W}{\partial p} - \frac{\hbar^2}{24} \frac{\partial^3 V}{\partial q^3} \frac{\partial^3 F^W}{\partial p^3} + \dots \quad (1.8)$$

The classical Liouville equation (1.7) can be efficiently solved with the *method of characteristics*, see e.g. Ref. [10], and this is also the basis of our QMD approach where an ensemble of “classical” (Wigner) trajectories is used to solve (numerically) the quantum Wigner-Liouville equation (1.4) which will be discussed in Sec. 1.4. The time-dependence of the trajectories is given by “classical” equations of motion

$$\frac{\partial q}{\partial t} = \frac{p}{m}, \quad \frac{\partial p}{\partial t} = -\frac{\partial V_{\text{eff}}(p, q, t)}{\partial q}, \quad (1.9)$$

Of course, a direct solution of Eq. (1.9) with the definition Eq. (1.8) is only useful if the series is rapidly converging and there is only a small number of non-zero terms.

However, there is also a principle difficulty with this approach, if the series of terms with the potential derivatives is not converging which is the case, e.g., for a Coulomb potential (at zero distance). There are at least three solutions. The first is to solve the Wigner-Liouville equation by using Monte Carlo techniques [11]–[14], which is discussed below in Section 1.4. The second is to replace the original potential on the r.h.s. of Eq. (1.8) by some model potential which has a finite number of nonzero derivatives as it is done e.g. in Ref. [15]. The third approach is to perform a suitable average of V_{eff} , e.g. over a thermal ensemble of particles. This has been done both for external potentials and also for two particle interaction. This latter case of an effective quantum pair potential and its use in classical MD is discussed in the next section.

1.3 Semiclassical MD simulation

Quantum pair potentials. In order to obtain an effective pair potential which is regularized at zero by quantum effects (finite at zero interparticle dis-

tance), we consider Eq. (1.4) for 2 particles. Assuming further thermodynamic equilibrium (with a given temperature $k_B T = 1/\beta$), spatial homogeneity and neglecting 3-particle correlations, one can solve for the two-particle Wigner function $F_{12}^W = F_{12}^{EQ}(r_1, p_1, r_2, p_2, \beta) \approx F_{12}^{EQ}(r_1 - r_2, p_1, p_2, \beta)$. This is now re-written as in the canonical case [7], $F_{12}^{EQ}(r_1 - r_2, p_1, p_2, \beta) \equiv F_1^{EQ}(p_1, \beta) F_2^{EQ}(p_2, \beta) e^{-\beta V_{12}^Q}$, which defines the desired quantum pair potential V_{12}^Q .

The first solution for V_{12}^Q was found by Kelbg in the limit of weak coupling [16] and has the form of Eq. (1.10) with $\gamma_{ij} \rightarrow 1$, for details and references, cf. [10, 17]. The Kelbg potential (or slightly modified versions) is widely used in numerical simulations of dense plasmas, e.g. [18, 19, 5, 20]. It is finite at zero distance correctly capturing basic quantum diffraction effects which prevent any divergence. However, the absolute value at $r = 0$ is incorrect which has lead to the derivation of further improved potentials, e.g. [21, 10, 17] and references therein. Here we use the *improved Kelbg potential* (IKP),

$$\Phi(r_{ij}, \beta) = \frac{q_i q_j}{r_{ij}} \left[1 - e^{-\frac{r_{ij}^2}{\lambda_{ij}^2}} + \sqrt{\pi} \frac{r_{ij}}{\lambda_{ij} \gamma_{ij}} \left(1 - \operatorname{erf} \left[\gamma_{ij} \frac{r_{ij}}{\lambda_{ij}} \right] \right) \right], \quad (1.10)$$

where $x_{ij} = |\mathbf{r}_{ij}|/\lambda_{ij}$, $\lambda_{ij}^2 = \frac{\hbar^2 \beta}{2\mu_{ij}}$ and $\mu_{ij}^{-1} = m_i^{-1} + m_j^{-1}$, which contains an additional free parameter γ_{ij} which can be obtained from a fit to the exact solution of the two-particle problem [17].

MD Simulations. We have performed extensive MD simulations of dense partially ionized hydrogen in thermodynamic equilibrium using different IKP for electrons with different spin projections. To properly account for the long-range character of the potentials, we used periodic boundary conditions with the standard Ewald procedure [3]. The number of electrons and protons was $N = 200$. Our MD simulations use standard Runge-Kutte or Verlet algorithms [3] to solve Newton's equations Eq. (1.9), where V_{eff} is replaced by the IKP. Because of the temperature dependence of the IKP we applied a temperature scaling at every time step for all components separately (for protons and two sorts of electrons) to guarantee a constant temperature of all components in our equilibrium simulations. In each simulation the system was equilibrated for at least 10^4 MD steps, only after this the observables have been computed.

In Fig. 1.1 we plot the internal energy per atom as a function of temperature for two densities and compare it to path integral Monte Carlo (PIMC) results [17, 22]. The density is given by the Bruckner parameter $r_s = \bar{r}/a_B$, where \bar{r} is average interparticle distance and a_B denotes the Bohr radius. For high temperatures and weak coupling, $\Gamma = e^2/(\bar{r}k_B T) < 1$ (fully ionized plasma), the two simulations coincide within the limits of statistical errors. If we use the original Kelbg potential, at temperatures below 300,000 K (approximately 2 times the binding energy), the MD results start to strongly deviate from the PIMC results. In contrast the IKP fully agrees the PIMC data even at temperatures far below the hydrogen binding energy Ry , where the plasma

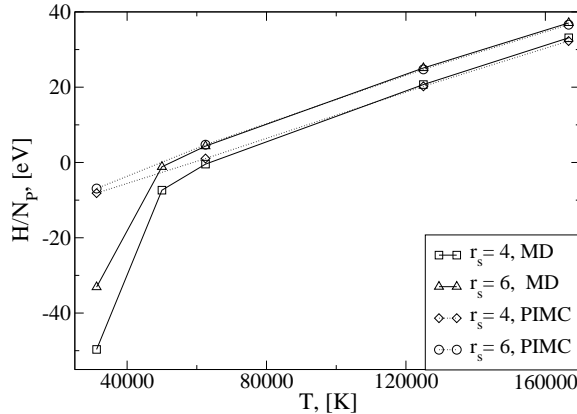


Fig. 1.1. Internal energy per hydrogen atom at $r_s = 4$ and $r_s = 6$ versus temperature, MD results are compared to restricted PIMC simulations [17, 22].

is dominated by atoms, which is a remarkable extension of ‘semiclassical’ MD into the theoretically very difficult regime of moderate coupling, moderate degeneracy and partial ionization.

Interestingly, even bound states can be analyzed in our simulations by following the electron trajectories. At $T < 1Ry$, we observe an increasing number of electrons undergoing strong deflection (large angle scattering) on protons and eventually performing quasi-bound trajectories. Most of these electrons remain “bound” only for a few classical orbits and then leave the proton again. Averaged over a long time, our simulations are able to reveal the degree of ionization of the plasma. For temperatures below approximately $50,000K$ (which is close to the binding energy of hydrogen molecules), the simulations cannot be applied. Although we clearly observe molecule formation (see below), there also appear clusters of several molecules which is unphysical in the present conditions and is caused by the approximate (two-particle) treatment of quantum effects in the IKP. This turns out to be the reason for the too low energy in Fig. 1.1 at low temperatures.

Let us now turn to a more detailed analysis of the spatial configuration of the particles. In Fig. 1.2 the pair distribution functions of all particle species with the same charge are plotted at two densities. Consider first the case of $T = 125,000$ K (upper panels). For both densities, all functions agree qualitatively, showing a depletion at zero distance due to Coulomb repulsion. Besides, there are differences which arise from the spin properties. Electrons with the same spin show a “Coulomb hole” around $r = 0$ which is broader than the one of the protons due to the Pauli principle (additional repulsion of electrons with the same spin projection). This trend is reversed at low temperatures, see the middle panel, which is due to the formation of hydrogen atoms and molecules. In this case, electrons (i.e., their classical trajectories) are “spread out” around the protons giving rise to an increased probability of close encounters of two electrons belonging to different atoms compared to two protons.

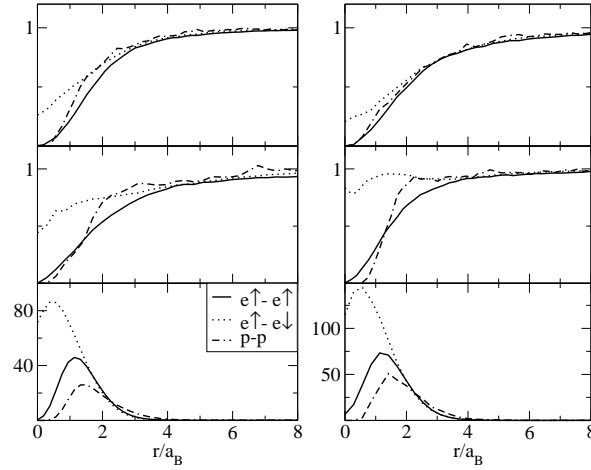


Fig. 1.2. Electron-electron and proton-proton pair distribution functions for a correlated hydrogen plasma with $r_s = 4$ (left row) and $r_s = 6$ (right row) for $T = 125,000K$, $61,250K$, and $31,250K$ (from top to bottom).

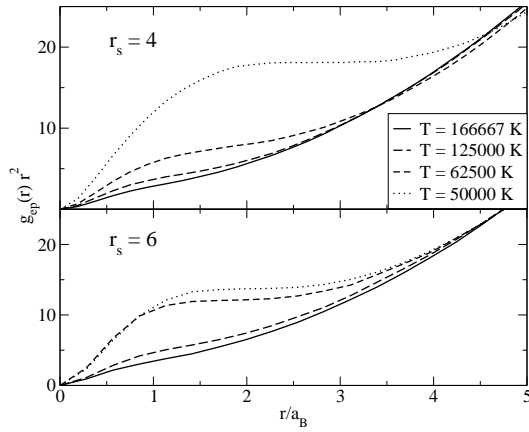


Fig. 1.3. Electron-proton pair distribution functions multiplied by r^2 as function of e-p distance at $r_s = 4$ (top) and $r_s = 6$ (bottom) and four temperatures.

Now, compare electrons with parallel vs. electrons with anti-parallel spins. In all cases, we observe a significantly increased probability to find two electrons with opposite spin at small distances below one Bohr radius which is due to the missing Pauli repulsion in this case. This trend increases with lowering of the temperature due to increasing quantum effects. Before analyzing the lowest temperature in Fig. 1.2 consider the electron-proton distributions. Multiplying these functions by r^2 gives essentially the radial probability density $W_{ep}(r) = r^2 g_{ep}(r)$, which is plotted in Fig. 1.3. At low temperatures this function converges to the ground state probability density of the hydrogen atom $W_{ep}(r) = r^2(r)|\psi|_{1s}^2(r)$ influenced by the surrounding plasma. Here, lowering of the temperature leads towards the formation of a shoulder around $1.4a_B$ for $r_s = 4$ and $1.2a_B$ for $r_s = 6$ which is due to the formation of hydrogen atoms (which is confirmed by the corresponding quasi-bound electron trajectories).

At this temperature, the observed most probable electron distance is slightly larger than one a_B as in the atom hydrogen ground state. Of course, classical MD cannot yield quantization of the bound electron motion, but it correctly reproduces (via averaging over the trajectories) the statistical properties of the atoms.

At 62, 500K and $r_s = 6$ (right center part of Fig. 1.2) the simulations show a first weak signature of molecule formation – see the maximum of the p-p distribution function around $r = 2a_B$ and the maximum of the distribution function of electrons with anti-parallel spins around $r = 1.5a_B$. Upon further lowering of the temperature by a factor of two (lower panel of Fig. 1.2) the p-p functions exhibit a clear peak very close to $r = 1.4a_B$ – the theoretical p-p separation in H_2 . At the same time, also the e-e functions have a clear peak around $r = 0.5a_B$ (the two electrons are concentrated between the protons). In contrast, in the case of parallel spins, no molecules are formed, the most probable electron distance is around $r = 1.2a_B$.

MD results for dynamic quantities. We now extend the analysis to the dynamic properties of an hydrogen plasma in equilibrium which is based on the fluctuation-dissipation theorem. The time-dependent microscopic density of plasma species α is defined as $\rho^\alpha(\mathbf{r}, t) = \sum_{i=1}^{N_\alpha} \delta[\mathbf{r} - \mathbf{r}_i^\alpha(t)]$, with the Fourier components $\rho^\alpha(\mathbf{k}, t) = \sum_{i=1}^{N_\alpha} \exp[i\mathbf{k} \cdot \mathbf{r}_i^\alpha(t)]$, where $\mathbf{r}_i(t)$ denotes the trajectory of particle “i” obtained in the simulation. We now define the three partial density-density time correlation functions (DDCF) between sorts α and η as

$$A^{\alpha\eta}(\mathbf{k}, t) = (N_\alpha + N_\eta)^{-1} \langle \rho^\alpha(\mathbf{k}, t) \rho^\eta(-\mathbf{k}, 0) \rangle, \quad (1.11)$$

where, due to isotropy, $\mathbf{k} = k$. Here $\langle \dots \rangle$, denotes averaging along the trajectories by shifting the time interval and keeping the difference equal to t . Note also, that $A^{\alpha\eta}(k, t) = A^{\eta\alpha}(k, t)$ for all pairs α and η . In addition to the spin-resolved electron functions we can also consider the spin averaged correlation function $A^e(k, t) = A^{\uparrow\uparrow}(k, t) + A^{\downarrow\downarrow}(k, t)$.

We have performed a series of simulation runs of equilibrium fluctuations in hydrogen plasmas with coupling parameters Γ and electron degeneracy parameters $\chi_e = \rho A_e^3$ with the electron DeBroglie wavelength $\Lambda_e = \hbar / \sqrt{2\pi m_e k_B T}$ ranging from zero (classical system) to one (quantum or “degenerate” system). The electron DDCF for $\Gamma = 1$ and $\chi_e = 1$ are plotted in Fig. 1.4 for four values of the dimensionless wavenumber, $q = k\bar{r}$. The correlation functions ($\uparrow\uparrow$ and $\downarrow\downarrow$) have two characteristic behaviors – a highly damped, high-frequency part and a weakly damped low-frequency tail. The latter is related to the slow ionic motion and the first one to oscillations with frequencies close to the electron plasma frequency ω_{pl} . On the other hand, the time scale of the ion motion is determined by the ion plasma frequency $\omega_{pl}^i = \sqrt{4\pi\rho_i Z_i^2 e^2 / m_i}$, their ratio being about 43 (square root of the ion-to-electron mass ratio). The slow proton oscillations are clearly seen in the proton DDCF, shown in Fig. 1.5. To resolve the proton oscillations the whole simulation (including the electron dynamics) has to extend over several proton plasma periods $T_p = 2\pi / \omega_{pl}^i$ thereby resolv-

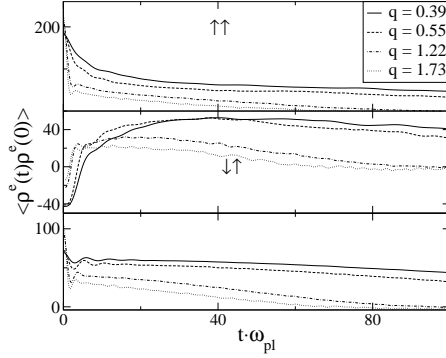


Fig. 1.4. Electron DDCF (1.11) multiplied by $(N_e^\uparrow + N_e^\downarrow)$ for $\Gamma = 1$ and $\chi_e = 1$ for four wave vectors. Upper (center) figure: correlation functions for parallel (antiparallel) spins, bottom figure: spin-averaged function.

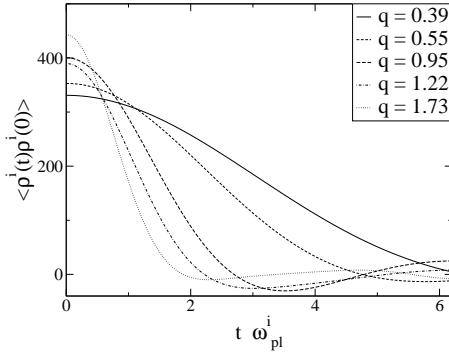


Fig. 1.5. Proton DDCF (1.11) for $\Gamma = 1$ and $\chi_e = 1$ for five wave vectors (in units of $1/\bar{r}$).

ing the fast electronic motions as well, which sets the numerical limitation of the calculation.

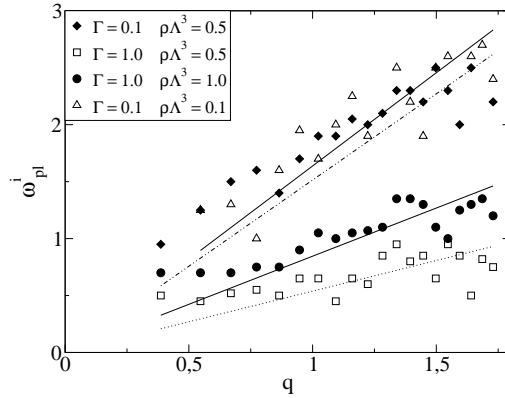


Fig. 1.6. Ion-acoustic wave dispersion in a dense hydrogen plasma. Lines correspond to weighted linear fits to the MD data (symbols). The scatter of the data is due to the limited particle number N and simulation time and can be systematically reduced. Also, smaller q -values require larger N .

The temporal Fourier transform of the DDCF yields another very important quantity – the *dynamic structure factor*, $S_{\alpha,\eta}(\omega, q)$, which allows one to analyze, e.g., the dispersion of the coupled electron and proton oscillations. Fig. 1.6 shows dispersion results for the collective proton oscillations (for the electron modes, see Refs. [20, 22]) which follow from the peak positions of $S_{ii}(\omega, q)$. Fig. 1.6 shows the peak frequency versus wave number, i.e. the dispersion of longitudinal ion-acoustic waves, $\omega(q) = v_{MD} \cdot q$, where v_{MD} denotes our MD result for the phase velocity. This can be compared to the

familiar analytical expression for an ideal two-temperature ($T_e \gg T_i$) plasma $v_s = \sqrt{Z_i k_B T_e / m_i}$, where v_s is the ion sound velocity. We observe deviations of about 10%, for weak degeneracy, $\chi_e < 0.5$, and about 10%, for large degeneracy, $\chi_e \geq 1$, which are due to nonideality (correlations) and quantum effects, directly included in our simulations. For further details on this method, see Refs. [22, 23, 6].

Thus the smicclassical MD is a powerful approach to correlated quantum plasmas. Thermodynamic and dynamic properties are accurately computed if accurate quantum pair potentials, such as the IKP, are being used.

1.4 Quantum dynamics

Now we discuss the method of Wigner trajectories in more detail. As we have seen, the Wigner function W [to avoid confusion, in this section we rename $F^W \rightarrow W$] in Eq. (1.2) is the Fourier transform of the non-diagonal elements of the density matrix which, for a pure state, is $\rho(q + \frac{p}{2}, q - \frac{p}{2}, t) \psi(q + \frac{p}{2}, t) \psi^*(q - \frac{p}{2}, t)$, where the N -particle wave functions satisfy the Schrödinger equation with an initial condition

$$i\hbar \frac{\partial \psi}{\partial t} = \hat{H} \psi; \quad \psi(t_0) = \psi^0(q), \quad (1.12)$$

which contains the hamiltonian (1.3) [recall that q is a vector of dimensionality $\{N \times d\}$]. By taking the time derivative of W in Eq. (1.2), substituting it in the l.h.s of the Schrödinger equation instead of $\partial \psi / \partial t$ and integrating by parts, we recover Eq. (1.4). For convenience of the further analysis, we separate the contribution of the classical force $\mathbf{F}(q) = -\nabla_q V(q)$, compensating it in the function ω which now replaces $\tilde{\omega}$,

$$\frac{\partial W}{\partial t} + \frac{\mathbf{p}}{m} \cdot \nabla_q W + \mathbf{F}(q) \cdot \nabla_p W = \int_{-\infty}^{\infty} ds W(p-s, q, t) \omega(s, q, t), \quad (1.13)$$

$$\omega(s, q, t) = \frac{2}{(\pi \hbar^2)^{Nd}} \int dq' V(q-q', t) \sin\left(\frac{2sq'}{\hbar}\right) + \mathbf{F}(q) \cdot \nabla_s \delta(s). \quad (1.14)$$

In the classical limit ($\hbar \rightarrow 0$), the r.h.s of Eq. (1.13) vanishes and we obtain the classical Liouville equation

$$\frac{\partial W}{\partial t} + \frac{\mathbf{p}}{m} \cdot \nabla_q W + \mathbf{F}(q) \cdot \nabla_p W = 0. \quad (1.15)$$

The solution of Eq. (1.15) is known and can be expressed by the Green function [9]

$$G(p, q, t; p_0, q_0, t_0) = \delta[p - \bar{p}(t; t_0, p_0, q_0)] \delta[q - \bar{q}(t; t_0, p_0, q_0)],$$

where $\bar{p}(\tau)$ and $\bar{q}(\tau)$ are the phase space trajectories (of all particles), which are the solutions of Hamilton's equations together with the initial conditions at $\tau = t_0 = 0$,

$$\begin{aligned} d\bar{q}/d\tau &= \bar{p}(\tau)/m; & \bar{q}(0) &= q_0, \\ d\bar{p}/d\tau &= \mathbf{F}(\bar{q}(\tau)); & \bar{p}(0) &= p_0. \end{aligned} \quad (1.16)$$

Using the Green function, the time-dependent solution of the classical Liouville equation takes the form

$$W(p, q, t) = \int dp_0 dq_0 G(p, q, t; p_0, q_0, 0) W_0(p_0, q_0). \quad (1.17)$$

With this result, it is now possible to construct a solution also for the quantum case. To this end we note that it is straightforward to convert Eq. (1.13) into an integral equation

$$\begin{aligned} W(p, q, t) &= \int dp_0 dq_0 G(p, q, t; p_0, q_0, 0) W_0(p_0, q_0) + \\ &\int_0^t dt_1 \int dp_1 dq_1 G(p, q, t; p_1, q_1, t_1) \int_{-\infty}^{\infty} ds_1 \omega(s_1, q_1, t_1) W(p_1 - s_1, q_1, t_1), \end{aligned} \quad (1.18)$$

which is exact and can be solved efficiently by iterations [11, 10]. First, we can express the function $W(p_1 - s_1, q_1, t_1)$ written on the r.h.s. of Eq. (1.18), formally, using the same Eq. (1.18) but written for another set of variables, i.e. $\{p, q, t\} \rightarrow \{p_1 - s_1, q_1, t_1\}$ and $\{p_1, q_1, s_1, t_1\} \rightarrow \{p_2, q_2, s_2, t_2\}$. Second, substitution of the obtained result again in Eq. (1.18) gives

$$\begin{aligned} W(p, q, t) &= W^{(0)}(p, q, t) + W^{(1)}(p, q, t) + \int_0^t dt_1 \int d1 G(p, q, t; 1, t_1) \times \\ &\int_0^{t_1} dt_2 \int d2 G(p_1 - s_1, q_1, t_1; 2, t_2) \int_{-\infty}^{\infty} ds_2 \omega(s_2, q_2, t_2) W(p_2 - s_2, q_2, t_2), \end{aligned} \quad (1.19)$$

where we have introduced the short notations $n \equiv q_n, p_n$, $dn \equiv dq_n dp_n$ and

$$W^{(0)}(p, q, t) = \int d0 G(p, q, t; 0, 0) W_0(0), \quad (1.20)$$

$$\begin{aligned} W^{(1)}(p, q, t) &= \int_0^t dt_1 \int_{-\infty}^{\infty} d1 G(p, q, t; 1, t_1) \int_{-\infty}^{\infty} ds_1 \omega(s_1, q_1, t_1) \\ &\times \int d0 G(p_1 - s_1, q_1, t_1; 0, 0) W_0(0). \end{aligned} \quad (1.21)$$

$W^{(0)}(p, q, t)$ (as it follows from the Green function $G(p, q, t; p_0, q_0, 0)$) describes the propagation of the Wigner function along the classical characteristics, i.e., the solutions of Hamilton's equations (1.16) in the time interval $[0, t]$. It is worth mentioning, that this first term describes both classical and quantum effects, due to the fact that the initial Wigner function $W_0(p_0, q_0)$, in general, contains all powers of Planck's constant \hbar contained in the initial state wave

functions. The second and third terms on the r.h.s. of Eq. (1.19) describe additional quantum corrections to the time evolution of $W(p, q, t)$.

Let us consider the term $W^{(1)}(p, q, t)$ in more detail. It was first proposed in Ref. [11] and demonstrated in Refs. [12]–[14] that the multiple integral (1.21) can be calculated stochastically by Monte Carlo techniques. For this we need to generate an ensemble of trajectories in phase space. To each trajectory we ascribe a specific weight, which gives its contribution to (1.21). For example, let us consider a trajectory which starts at point $\{p_0, q_0, \tau = 0\}$. This trajectory acquires a weight equal to the value $W_0(p_0, q_0)$. Up to the time $\tau = t_1$ the trajectory is defined by the Green function $G(p_1 - s_1, q_1, t_1; p_0, q_0, 0)$. At $\tau = t_1$, as it follows from Eq. (1.21), the weight of this trajectory must be multiplied by the factor $\omega(s_1, q_1, t_1)$, and simultaneously a perturbation in momentum takes place: $(p_1 - s_1) \rightarrow p_1$. As a result the trajectory becomes discontinuous in momentum space (but continuous in the coordinate space). This is, obviously, a manifestation of the Heisenberg uncertainty of coordinates and momenta. Now, the trajectory consists of two parts – two classical trajectories which are the solutions of Eq. (1.16), which are separated, at $\tau = t_1$, by a “momentum jump” of magnitude s_1 . What about the value s_1 of the jump and the time instance t_1 ? Both appear under integrals with a certain probability. To sample this probability adequately, a statistical ensemble of trajectories should be generated, further the instant of time t_1 must be chosen randomly in the interval $[0, t]$, and the momentum jump s_1 randomly in the interval $(-\infty, +\infty)$. Finally, also different starting points $\{p_0, q_0\}$ of trajectories at $\tau = 0$ must be considered (due to the integration $\int dp_0 dq_0$). Considering a sufficiently large number of trajectories of such type we can accurately calculate $W^{(1)}(p, q, t)$ – the first correction to the classical evolution of the quantum distribution function $W^{(0)}(p, q, t)$.

Let us now take into account the third term in Eq. (1.19). We now substitute, instead of $W(p_2 - s_2, q_2, t_2)$, its integral representation, using (1.18). As a result we get, for this term,

$$\begin{aligned} W^{(2)}(p, q, t) = & \int_0^t dt_1 \int d1G(p, q, t; 1, t_1) \int_{-\infty}^{\infty} ds_1 \omega(s_1, q_1, t_1) \times \\ & \int_0^{t_1} dt_2 \int d2G(p_1 - s_1, q_1, t_1; 2, t_2) \int_{-\infty}^{\infty} ds_2 \omega(s_2, q_2, t_2) \times \\ & \int d0G(p_2 - s_2, q_2, t_2; 0, 0) W_0(0). \end{aligned} \quad (1.22)$$

If we apply the stochastic interpretation of the integrals, as we did above for $W^{(1)}(p, q, t)$, this term can be analogously calculated using an ensemble of classical trajectories with *two* momentum jumps taking place at time instants $\tau = t_1$ and $\tau = t_2$, and with a weight function multiplied by the factors $\omega(s_1, q_1, t_1)$ and $\omega(s_2, q_2, t_2)$, respectively.

Applying the above procedure several times, we can get the higher order correction terms. As a result, $W(p, q, t)$ will be expressed as an iteration series,

with each term of the series representing a contribution of trajectories of a definite topological type – with *one, two, three, etc.* momentum jumps. In Fig. 1.7 we show an example of trajectories contributing to the terms $W^{(0)}, W^{(1)}$ and $W^{(2)}$.

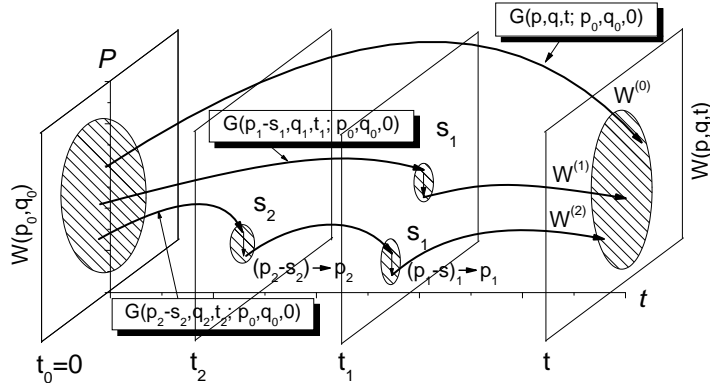


Fig. 1.7. Illustration of the iteration series. Three types of trajectories are shown: without (top curve), with one (middle) and two (lower) momentum jumps.

As was noted in Section 1.2 the Wigner function allows us to compute quantum-mechanical expectation values of an arbitrary one-particle operator \hat{A} . Using the idea of the iteration series (1.19), we obtain an iteration series also for the expectation value,

$$\langle \hat{A} \rangle(t) = \int dpdq A(p, q)W(p, q, t) = \langle \hat{A} \rangle^{(0)}(t) + \langle \hat{A} \rangle^{(1)}(t) + \dots, \quad (1.23)$$

where different terms correspond to different terms in the series for W . The series (1.23) maybe computed much more efficiently than the one for W since the result does not depend on coordinates and momenta anymore.

Certainly, in the iteration series it is possible to take into account only a finite number of terms and contributions of a limited number of trajectories. Interestingly, it is not necessary to compute the individual terms iteratively. Instead, all (relevant) terms can be calculated simultaneously using the basic concepts of Monte Carlo methods, e.g. [24]. An important task of the Monte Carlo procedure will be to generate stochastically mostly the trajectories which give the dominant contribution to the result, for details, see [10].

1.5 Time correlation functions in the canonical ensemble

So far we have considered the dynamics of pure states where the density matrix ρ is defined by a single wavefunction ψ . However, at finite temperature ρ is, in general, defined by an incoherent superposition of wave functions (mixed

states). Here we consider a canonical ensemble as the most common one. Time correlation functions $C_{FA}(t) = \langle F(0)A(t) \rangle$ are among the most important quantities in Statistical physics which describe transport properties, such as diffusion, dielectric properties, chemical reaction rates, equilibrium and non-equilibrium optical properties, etc. An example has already been considered in Sec. 1.3 – the density-density auto-correlation function (1.11). Here, we use a more general expression for the quantum correlation function of two quantities A and F given by the operators \hat{F} and \hat{A} . In the canonical ensemble the averaging is performed by a trace with the canonical density operator $\hat{\rho}^{EQ} = Z^{-1}e^{-\beta\hat{H}}$, with $\beta = 1/k_B T$, and the correlation function has the form [25]

$$C_{FA}(t) = \frac{1}{Z} \text{Tr}(\hat{F} e^{i\hat{H}t_\beta^*} \hat{A} e^{-i\hat{H}t_\beta}), \quad (1.24)$$

where \hat{H} is the Hamiltonian (1.3), t_β is a complex time argument (it “absorbs” $\hat{\rho}^{EQ}$), $t_\beta = t - i\beta/2$, $Z = \text{Tr}\rho^{EQ}$ is the partition function, and we use $\hbar = 1$.

The time correlation function can now be computed by first, writing Eq. (1.24) in coordinate representation and then transforming to the Wigner picture using the Weyl representation of \hat{F} and \hat{A} ,

$$\begin{aligned} C_{FA}(t) &= \\ & Z^{-1} \int dq_1 dq_2 dq_3 dq_4 \langle q_1 | \hat{F} | q_2 \rangle \langle q_2 | e^{i\hat{H}t_\beta^*} | q_3 \rangle \langle q_3 | \hat{A} | q_4 \rangle \langle q_4 | e^{-i\hat{H}t_\beta} | q_1 \rangle \\ &= \int dp_1 dq_1 dp_2 dq_2 F(p_1, q_1) A(p_2, q_2) W(p_1, q_1; p_2, q_2; t; \beta), \end{aligned} \quad (1.25)$$

where $W(p_1, q_1; p_2, q_2; t; \beta)$ is now a generalization of the Wigner function which is defined as double Fourier transformation of the product of two non-diagonal matrix elements of the density operator

$$\begin{aligned} W(p_1, q_1; p_2, q_2; t; \beta) &= \frac{1}{Z(2\pi)^{2Nd}} \int d\xi_1 d\xi_2 e^{ip_1\xi_1} e^{ip_2\xi_2} \times \\ & \left\langle q_1 - \frac{\xi_1}{2} \left| e^{i\hat{H}t_\beta^*} \right| q_2 + \frac{\xi_2}{2} \right\rangle \left\langle q_2 - \frac{\xi_2}{2} \left| e^{-i\hat{H}t_\beta} \right| q_1 + \frac{\xi_1}{2} \right\rangle. \end{aligned} \quad (1.26)$$

Calculating the partial time derivatives of the function W using the usual technique for matrix elements, it can be shown that the function W satisfies a system of two Wigner-Liouville equations [12, 13]

$$\begin{aligned} \frac{\partial W}{\partial t} + \frac{\mathbf{p}_1}{m} \cdot \nabla_{\mathbf{q}_1} W + \mathbf{F}(\mathbf{q}_1) \cdot \nabla_{\mathbf{p}_1} W &= I_1, \\ \frac{\partial W}{\partial t} + \frac{\mathbf{p}_2}{m} \cdot \nabla_{\mathbf{q}_2} W + \mathbf{F}(\mathbf{q}_2) \cdot \nabla_{\mathbf{p}_2} W &= I_2, \end{aligned} \quad (1.27)$$

where on the r.h.s. we have two “collison” integrals

$$\begin{aligned}
I_1 &= \int_{-\infty}^{\infty} ds_1 W(p_1 - s_1, q_1; p_2, q_2; t; \beta) \omega(s_1, q_1, t) \\
I_2 &= \int_{-\infty}^{\infty} ds_2 W(p_1, q_1; p_2 - s_2, q_2; t; \beta) \omega(s_2, q_2, t), \quad (1.28)
\end{aligned}$$

and the function $\omega(s, q, t)$ is defined in the same way as in the microcanonical ensemble, see Eq. (1.14).

1.5.1 Initial conditions for the Wigner-Liouville equation

Using Eq. (1.26) at $t = 0$, we find that the initial value of the Wigner function is given by the integral (again $1 = q_1, p_1$)

$$\begin{aligned}
W_0(1; 2; 0; \beta) &= \frac{1}{Z(2\pi)^{2Nd}} \int d\xi_1 d\xi_2 e^{ip_1\xi_1} e^{ip_2\xi_2} \\
&\left\langle q_1 - \frac{\xi_1}{2} \left| e^{-\beta\hat{H}/2} \right| q_2 + \frac{\xi_2}{2} \right\rangle \left\langle q_2 - \frac{\xi_2}{2} \left| e^{-\beta\hat{H}/2} \right| q_1 + \frac{\xi_1}{2} \right\rangle. \quad (1.29)
\end{aligned}$$

Let us now use the group property of the density operator $\hat{\rho}$ and the high temperature approximation for the matrix elements of $\langle q' | \hat{\rho} | q \rangle$ [26],

$$\begin{aligned}
e^{-\beta\hat{H}} &= \left[e^{-\frac{\beta}{M}\hat{H}} \right]^M \\
\langle q' | e^{-\frac{\beta}{2M}\hat{H}} | q'' \rangle &\approx \langle q' | e^{-\frac{\beta}{2M}\hat{K}} | q'' \rangle \langle q' | e^{-\frac{\beta}{2M}\hat{U}} | q'' \rangle. \quad (1.30)
\end{aligned}$$

As a result, we obtain

$$\begin{aligned}
W_0(1; 2; 0; \beta) &\approx \frac{1}{Z(2\pi\hbar)^{2Nd}} \int dq'_1 \dots dq'_M dq''_1 \dots dq''_M e^{-\sum_{m=2}^M K_m - \sum_{m=1}^M U_m} \times \\
&\int d\xi_1 e^{ip_1\xi_1/\hbar} \left\langle q'_M \left| e^{-\frac{\beta}{2M}\hat{K}} \right| q_1 + \frac{\xi_1}{2} \right\rangle \left\langle q_1 - \frac{\xi_1}{2} \left| e^{-\frac{\beta}{2M}\hat{K}} \right| q''_1 \right\rangle \times \\
&\int d\xi_2 e^{ip_2\xi_2/\hbar} \left\langle q''_M \left| e^{-\frac{\beta}{2M}\hat{K}} \right| q_2 + \frac{\xi_2}{2} \right\rangle \left\langle q_2 - \frac{\xi_2}{2} \left| e^{-\frac{\beta}{2M}\hat{K}} \right| q''_1 \right\rangle, \quad (1.31)
\end{aligned}$$

where

$$K_m = \frac{\pi}{\lambda_M^2} [(q'_m - q'_{m-1})^2 + (q''_m - q''_{m-1})^2], \quad U_m = \frac{\beta}{2M} [U(q'_m) + U(q''_m)].$$

Here we have assumed that $M \gg 1$, and $\lambda_M^2 = \frac{2\pi\hbar^2\beta}{mM}$ denotes the thermal de Broglie wave length corresponding to the inverse temperature $\frac{\beta}{2M}$. A direct calculation of the last two factors in Eq. (1.31) gives

$$\begin{aligned}
&\int d\xi_1 e^{ip_1\xi_1/\hbar} \left\langle q'_M \left| e^{-\frac{\beta}{2M}\hat{K}} \right| q_1 + \frac{\xi_1}{2} \right\rangle \left\langle q_1 - \frac{\xi_1}{2} \left| e^{-\frac{\beta}{2M}\hat{K}} \right| q''_1 \right\rangle \\
&= \left\langle q'_M \left| e^{-\frac{\beta}{2M}\hat{K}} \right| q \right\rangle \phi(p; q'_M, q_1) \left\langle q \left| e^{-\frac{\beta}{2M}\hat{K}/2M} \right| q_1 \right\rangle, \quad (1.32)
\end{aligned}$$

where

$$\phi(p; q'_M, q_1) = (2\lambda_M^2)^{Nd/2} \exp\left(-\frac{(p\lambda_M/\hbar + i\pi(q' - q'')/\lambda_M)^2}{2\pi}\right). \quad (1.33)$$

The final result for the Wigner function at $t = 0$ can be written as

$$\begin{aligned} W(1; 2; 0; \beta) &\approx \\ &\int dq'_1 \dots dq'_M dq''_1 \dots dq''_M \Psi(1; 2; q'_1 \dots q'_M; q''_1 \dots q''_M; 0; \beta) \times \\ &\phi(p_2; q'_M, q''_1) \phi(p_1; q''_M, q'_1), \end{aligned} \quad (1.34)$$

where

$$\Psi(p_1, q_1; p_2, q_2; q'_1 \dots q'_M; q''_1 \dots q''_M; \beta) = Z^{-1} e^{-\sum_{m=1}^{M+1} K_m - \sum_{m=1}^M U_m}.$$

Here we have introduced the notation $\{q'_0 \equiv q_1; q''_0 \equiv q_2\}$ and $\{q'_{M+1} \equiv q_2; q''_{M+1} \equiv q_1\}$. The Fig. 1.8 is an illustration of the simulation idea. Two closed loops with the set of points show the path integral representation of the density matrices in Eq. (1.31). The left chain of points, i.e.

$\{q_1, q'_1, \dots, q'_M, q_2, q''_1, \dots, q''_M\}$ characterizes the “path” of a single quantum particle. The chain has two special points (p_1, q_1) and (p_2, q_2) . As it follows from Eqs. (1.26), (1.27), these points are the original points for the Wigner function (the additional arguments arise from the path integral representation). As we show in the next section, we can consider these points as starting points for two dynamical trajectories propagating forward and backward in time, i.e. $t \rightarrow t^+$ and $t \rightarrow t^-$. The Hamilton equations for the trajectories are defined in the next section.

1.5.2 Integral equations

The solution scheme follows the one explained before. The only difference is that we now have to propagate two trajectories instead of one,

$$\begin{aligned} \frac{d\bar{q}_1}{d\tau} &= \frac{\bar{p}_1(\tau)}{2m}; & \bar{q}_1(0) &= q_1^0 \\ \frac{d\bar{p}_1}{d\tau} &= \frac{1}{2} \mathbf{F}[\bar{q}_1(\tau)]; & \bar{p}_1(0) &= p_1^0 \\ \frac{d\bar{q}_2}{d\tau} &= -\frac{\bar{p}_2(\tau)}{2m}; & \bar{q}_2(0) &= q_2^0 \\ \frac{d\bar{p}_2}{d\tau} &= -\frac{1}{2} \mathbf{F}[\bar{q}_2(\tau)]; & \bar{p}_2(0) &= p_2^0. \end{aligned} \quad (1.35)$$

the first (second) propagating forward (backward) Let us substitute expressions for $\mathbf{F}[\bar{q}_1(\tau)]$, $\bar{p}_1(\tau)$, $\mathbf{F}[\bar{q}_2(\tau)]$ and $\bar{p}_2(\tau)$ from (1.35) into Eqs. (1.27) and subtract the second equation from the first. As a result, in the l.h.s. we will

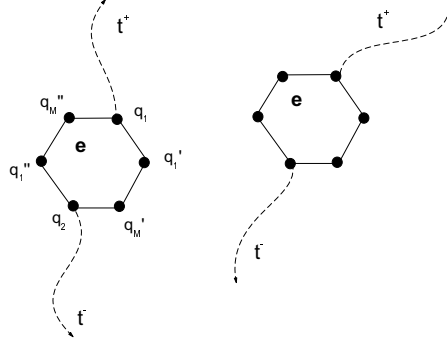


Fig. 1.8. Two closed loops illustrating the path integral representation of two electrons in the density matrices in Eq. (1.31), see also Ref. [26]. Two special points (p_1, q_1) and (p_2, q_2) are starting points for two dynamical trajectories propagating forward and backward in time.

obtain a full differential of the Wigner function. After multiplication by the factor $\{1/2\}$ and integration over time, the integral equation for the Wigner function takes the form

$$\begin{aligned}
& W(p_1, q_1; p_2, q_2; t; \beta) = \\
& = \int dp_1^0 dq_1^0 dp_2^0 dq_2^0 G(p_1, q_1, p_2, q_2, t; p_1^0, q_1^0, p_2^0, q_2^0, 0) W(p_1^0, q_1^0; p_2^0, q_2^0; 0; \beta) + \\
& \int_0^t d\tau \int dp_1^1 dq_1^1 dp_2^1 dq_2^1 G(p_1, q_1, p_2, q_2, t; p_1^1, q_1^1, p_2^1, q_2^1, \tau) \times \\
& \int_{-\infty}^{\infty} ds d\eta \vartheta(s, q_1^1; \eta, q_2^1; \tau) W(p_1^1 - s, q_1^1; p_2^1 - \eta, q_2^1; \tau; \beta), \quad (1.36)
\end{aligned}$$

where $\vartheta(s, q_1^1; \eta, q_2^1; \tau) = \frac{1}{2} \{ \omega(s, q_1^1) \delta(\eta) - \omega(\eta, q_2^1) \delta(s) \}$. The dynamical Green function G is defined as

$$\begin{aligned}
& G(p_1, q_1, p_2, q_2, t; p_1^0, q_1^0, p_2^0, q_2^0, 0) = \delta\{p_1 - \bar{p}_1(\tau; p_1^0, q_1^0, 0)\} \times \\
& \delta\{q_1 - \bar{q}_1(\tau; p_1^0, q_1^0, 0)\} \cdot \delta\{p_2 - \bar{p}_2(\tau; p_2^0, q_2^0, 0)\} \cdot \delta\{q_2 - \bar{q}_2(\tau; p_2^0, q_2^0, 0)\} \quad (1.37)
\end{aligned}$$

Let us denote the first term on the r.h.s. of Eq. (1.36) as $W^{(0)}(p_1, q_1; p_2, q_2; t; \beta)$. This term represents the Wigner function of the initial state propagating along classical trajectories (characteristics), solutions of Eqs. (1.35). Using the same approach which was applied in the microcanonical ensemble, we obtain expressions for

$$W^{(1)}(p_1, q_1; p_2, q_2; t; \beta), W^{(2)}(p_1, q_1; p_2, q_2; t; \beta), \dots$$

and represent $W(p_1, q_1; p_2, q_2; t; \beta)$ as an iteration series. In this case, we can calculate this also with an ensemble of trajectories using the Quantum-Dynamics-Monte-Carlo approach which was described in [27]. As a result the

expression for the time correlation function (1.25) can be rewritten as

$$\begin{aligned} C_{FA}(t) &= \int dp_1 dq_1 dp_2 dq_2 F(p_1, q_1) A(p_2, q_2) W(p_1, q_1; p_2, q_2; t; \beta) = \\ &= \left(\phi(P) | W^{(0)}(P; \beta) \right) + \sum_{i=1}^{\infty} \left(\phi(P) | W^{(i)}(P; \beta) \right), \end{aligned} \quad (1.38)$$

where $(\dots | \dots)$ denotes the integral in the (now $2N$ -particle) phase space $\{p_1, q_1, p_2, q_2\}$, and $\phi(P) = F(p_1, q_1) A(p_2, q_2)$.

An illustrative example for the calculations of the time correlation functions C_{FA} is the momentum-momentum autocorrelation functions $C_{PP}(t)$ for a one-dimensional system of interacting electrons in an array of fixed random scatterers at finite temperature [27]. This system is of high interest because at zero temperature it shows Anderson localization if electron-electron (e-e) interaction is neglected. It has been a long standing of the question what the effect of e-e interaction on localization will be. The present method [27] is well suited to answer this question, and it could be shown that Coulomb e-e interaction enhances the mobility of localized electrons [27, 10].

1.6 Discussion

We have presented a general idea how to extend the powerful method of molecular dynamics to quantum systems. First, we discussed “semiclassical MD”, i.e., classical MD with accurate quantum pair potentials. This method is very efficient and allows to compute thermodynamic properties of partially ionized plasmas for temperatures above the molecule binding energy (i.e. as long as three and four particle correlations can be neglected). Further, frequency dependent quantities (e.g., plasmon spectrum) are computed correctly for $\omega < \omega_{pl}$. Further progress is possible if more general quantum potentials are derived.

In the second part, we considered ways to rigorously solve the quantum Wigner-Liouville equation for the N -particle Wigner function. Results were derived for both, a pure quantum state and a mixed state (canonical ensemble). Although this method is by now well formulated, it is still very CPU time costly, so that practical applications are only starting to emerge. Yet, we expect that, due to its first principle character, Wigner function QMD will become increasingly important for a large variety of complex many-body problems.

This work is supported by the Deutsche Forschungsgemeinschaft via SFB-TR 24 and in part by Award No. Y2-P-11-02 of the U.S. Civilian Research and Development Foundation for the Independent States of the Former Soviet Union (CRDF) and of Ministry of Education and Science of Russian Federation, and RF President Grant NS-3683.2006.2 for governmental support of leading scientific schools.

References

1. M.P. Allen and D.J. Tildesley, *Computer Simulations of Liquids*. Clarendon Press, Oxford, 1987.
2. Daan Frenkel and Berend Smit, *Understanding Molecular Simulations: From Algorithms to Applications*. Academic Press 2002.
3. see also the chapters on classical MD in this book.
4. H. Feldmeier and J. Schnack, *Rev. Mod. Phys.* **72**, 655 (2000).
5. D. Klakow, C. Toepffer, and P.-G. Reinhard, *Phys. Lett. A* **192**, 55 (1994); *J. Chem. Phys.* **101**, 10766 (1994).
6. G. Zwicknagel, and T. Pschiwul, *J. Phys. A: Math. General* **39** 4359 (2006)
7. M. Bonitz, "Quantum Kinetic Theory", B.G. Teubner, Stuttgart/Leipzig, 1998.
8. E. Wigner, *Phys. Rev.* **40**, 749 (1932).
9. V.I. Tatarsky, *Sov. Phys. Usp.* **139**, 4, 587 (1983).
10. Introduction to Computational Methods in Many Body Physics M. Bonitz, D. Semkat (eds.). Princeton: Rinton Press. 2006.
11. V.S. Filinov, Yu. Medvedev, V. Kamskyi, *Jour. Mol. Phys.* **85**, 717 (1995).
12. V.S. Filinov, *Jour. Mol. Phys.* **88**, 1517, 1529 (1996).
13. V.S. Filinov, Yu. Lozovik, A. Filinov, E. Zakharov, and A. Oparin, *Physica Scripta* **58**, 297, 304 (1998).
14. Yu.E. Lozovik and A. Filinov, *Sov. Phys. JETP*, **88**, 1026 (1999)
15. Yu.E. Lozovik, A.V. Filinov, and A.S. Arkhipov, *Phys. Rev. E* **67**, 026707 (2003).
16. G. Kelbg, *Ann. Physik*, **12**, 219 (1963); **13**, 354; **14**, 394 (1964).
17. A. Filinov, V. Golubnychiy, M. Bonitz, W. Ebeling, and J.W. Dufty, *Phys. Rev. E* **70**, 046411 (2004).
18. J.P. Hansen, and I.R. McDonald, *Phys. Rev. A* **23**, 2041-59 (1981).
19. V.S. Filinov, M. Bonitz, W. Ebeling, and V.E. Fortov, *Plasma Physics and Controlled Fusion* **43**, 743 (2001).
20. V. Golubnychiy, M. Bonitz, D. Kremp, and M. Schlanges, *Phys. Rev. E* **64**, 016409 (2001).
21. H. Wagenknecht, W. Ebeling, and A. Förster, *Contrib. Plasma Phys.* **41**, 15 (2001).
22. V.O. Golubnychiy, *Molecular Dynamics simulations of strongly correlated mesoscopic and macroscopic Coulomb systems*, PhD thesis, Kiel University (2004).
23. M. Bonitz, A. Filinov, V. Golubnychiy, Th. Bornath, and W.D. Kraeft, *Contrib. Plasma Phys.* 5-6, 450 (2005)
24. I.M. Sobol, *The Monte Carlo Method (Popular Lectures in Mathematics*, University of Chicago Press, 1975; [German translation:] I.M. Sobol, *Die Monte-Carlo-Methode*. Berlin, Dt. Verl. der Wiss., 1991.
25. D.N. Zubarev, *Nonequilibrium Statistical Thermodynamics*, Plenum Press, New York/London 1974.
26. see the chapter on path integral Monte Carlo by A. Filinov et al.
27. V. Filinov, P. Thomas, I. Varga, T. Meier, M. Bonitz, V. Fortov, and S.W. Koch *Phys. Rev. B* **65**, 165124 (2002).